Operational experience of a 500 kV photoemission gun

Nobuyuki Nishimori*
National Institutes for Quantum and Radiological Science and Technology, 1-1-1 Kouto, Sayo, Hyogo 679-5148, Japan

Ryoji Nagai and Ryoichi Hajima
National Institutes for Quantum and Radiological Science and Technology, Tokai, Naka, Ibaraki 319-1106, Japan

Masahiro Yamamoto, Yosuke Honda, Tsukasa Miyajima, and Takashi Uchiyama
High Energy Accelerator Research Organization (KEK), Oho, Tsukuba, Ibaraki 305-0801, Japan

(Received 26 February 2019; published 14 May 2019)

Operational experience of a 500 kV photoemission gun at the compact energy recovery linac (cERL) of the High Energy Accelerator Research Organization is presented. The gun, developed at the Japan Atomic Energy Agency, was found to have failures in two out of the ten-segment ceramic insulator just after installation at cERL. The gun had been operated at 390 kV with eight segments until April 2015 and provided a 0.9 mA beam. An additional two-segment insulator was installed on the top of the existing insulators to recover the high-voltage performance. The gun was then conditioned up to 539 kV and has been operated stably at 500 kV. No discharge caused by the gun itself was observed at 500 kV once the high threshold voltage for stable operation exceeded 500 kV. A dark current of a few picoamperes was generated at 500 kV from a photocathode puck with a semiconducting wafer, while no dark current was observed without a semiconducting wafer. Stable generation of a 500 keV beam with current greater than 0.8 mA was demonstrated for more than two hours.

DOI: 10.1103/PhysRevAccelBeams.22.053402

I. INTRODUCTION

Future megahertz-repetition rate x-ray free electron lasers (XFELs), high power FELs for extreme ultraviolet (EUV) lithography, and high luminosity electron ion colliders require high-brightness and high-current electron guns [1–5]. A dc photoemission gun with a GaAs or alkali antimonide photocathode is one of the most promising candidates for such guns, as demonstrated by the Cornell photoinjector, which employs a 400 kV gun, with emittance that satisfies the requirements of the high repetition rate XFEL LCLS-II [6] with highest average current 65 mA [7]. Further increase of the gun voltage is desirable to reduce space charge induced emittance growth, especially for high bunch charge operation [8,9].

We have developed a dc high voltage photoemission gun for energy recovery linac (ERL) light sources in Japan [10] and demonstrated generation of a 500 keV electron beam from the dc gun at the Japan Atomic Energy Agency (JAEA) [11]. This demonstration was achieved by solving two electrical discharge problems, one of which is discharge impinging on the ceramic surface of the insulator caused by field emission generated from a central stem electrode. We have employed a segmented insulator with guard rings to protect the insulator from the field emission and demonstrated application of 500 kV for 8 h with no discharge [12]. The other problem is high-voltage (HV) prebreakdown between the cathode and the gun vacuum chamber wall, including an anode. We have solved this problem by optimization of the accelerator gap length for 500 kV operation [13].

The gun was installed at the compact ERL (cERL) of the High Energy Accelerator Research Organization (KEK) in Oct. 2012 and a stable beam has been delivered since April 2013. The details of the cERL accelerator system are described elsewhere [10,14]. However, the operational voltage of the gun was limited to 390 kV until recently. This is because failures of two out of the ten-segment ceramic insulator were found at KEK after shipment of the gun from JAEA. The gun insulator was operated with eight segments during the commissioning instead of the full ten segments by connecting shorting bars between the electrodes of the failed segments.

*nishimori.nobuyuki@qst.go.jp

ERL operation up to 0.9 mA was demonstrated with this gun configuration.

In July 2015, an additional two-segment insulator was installed on the top of the existing insulator to recover 500 kV operation. HV conditioning was performed without the stem electrode and 539 kV was reached within 1 h. A holding test at 539 kV was then conducted with no discharge activity for more than 3 h [15]. This result clearly shows that the eight- plus two-segment ceramic insulator is functional. HV conditioning was performed with the stem electrode and cathode in place, and 537 kV operation was reached in 155 h, after which a HV holding test was conducted at 490 kV for more than 4 h in Dec. 2015. The HV threshold for stable operation in the dc electron gun was determined during the conditioning process [16].

In 2016, an additional 50 h of conditioning was performed and the HV threshold exceeded 500 kV. However, dark current was generated around the photocathode and the operational voltage was limited to 450 kV. The dark current was clearly detected with a radiation monitor and was generated when the photocathode puck was not properly mounted in the holder of the cathode. Proper installation of the photocathode puck finally suppressed the dark current to less than a few picoamperes. The gun was operated at 500 kV at the cERL for more than 200 h and generation of a 500 keV beam with a current greater than 0.8 mA was demonstrated for 2 h.

Here, we present our operational experience of the 500 kV photoemission gun at the cERL. The original gun configuration developed at JAEA is briefly described in Sec. II. In Sec. III, gun operation at the cERL is described. Operation with the eight-segment ceramic insulator at 390 kV is detailed in Sec. III A. Installation of the additional two-segment ceramic insulator on the existing ten-segment insulator is described in Sec. III B. The experimental results of HV conditioning with the additional ceramics are presented in Sec. III C. Application of HV even below the threshold voltage was found to facilitate an increase of the threshold level. The dark current measurement at 500 kV is described in Sec. III D, and the beam generation test at 500 kV is presented in Sec. IV. Finally, a summary is given in Sec. V.

II. 500 kV PHOTOEMISSION GUN

A 500 kV photoemission gun developed at JAEA was installed at the cERL in 2012. Figure 1 shows a schematic illustration of the gun. A GaAs wafer on a molybdenum puck is used as a photocathode. The wafer is prepared at the preparation chamber, where cesium and oxygen are alternatively applied for negative electron affinity activation. The activated cathode is then transferred to the cathode electrode in the gun HV chamber. The photoemission beam is accelerated by a static electric field applied between the cathode and anode electrodes. During HV conditioning, the

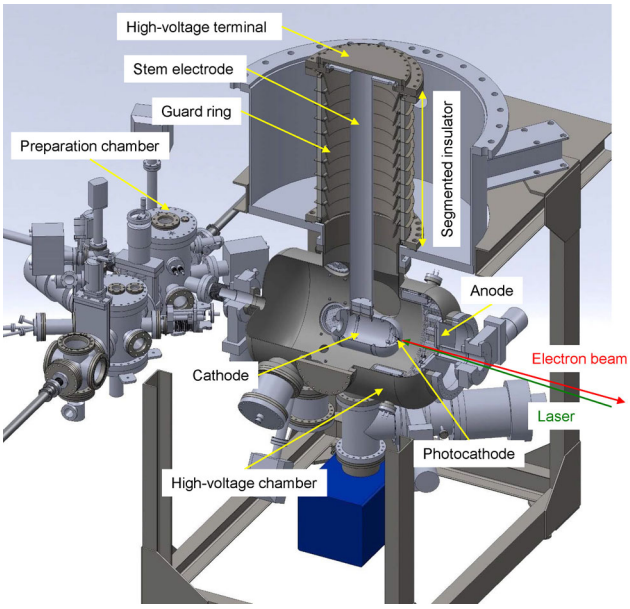

FIG. 1. Schematic illustration of the 500 kV dc photoemission gun developed at JAEA.

GaAs photocathode is replaced with a dummy puck made of stainless steel to avoid damage due to discharges. The details of the gun system have been described in Refs. [11–13,17].

A ceramic insulator with ten segments and guard rings was originally employed to reach HV without inducing fatal damage to the insulator by protecting the ceramics from field emission. HV conditioning up to 539 kV with the stem electrode was achieved in 2009 [12], and generation of a 500 keV beam with current up to 1.8 mA was demonstrated for short duration less than a minute in 2012 [11]. The cathode-anode gap length was changed from the original design of 100 mm to 160 mm [13] because field emitters that could not be pacified were created repeatedly with a 100 mm gap, which prevented stable gun operation at 500 kV.

The HV chamber, cathode, anode, and stem electrode are made of chemically polished (*CP*) titanium because the measured outgassing rate of *CP* titanium is much smaller than that of stainless steel [18], and the field emission current from titanium is lower than that from stainless steel [19]. The acceleration gap between the cathode and anode is surrounded by twenty 400 L/s nonevaporable getter (NEG) pumps to reduce residual gas. These NEG pumps are covered with HV shields made of 1 mm diameter titanium wire mesh. Three ICF203 ports of the HV chamber are used to install three 2000 L/s NEG pumps. In total, the HV chamber is equipped with 14000 L/s of NEG pumps. A 200 L/s ion pump pumps noble gases and methane. A 1000 L/s turbo molecular pump (TMP) is used during baking and HV conditioning. The base pressure of the HV chamber before HV conditioning is 0.8×10^{-9} Pa (N_2 equivalent), as measured

with an extractor gauge. A hot cathode vacuum gauge (Pfeiffer PBR260) was also used for high speed data acquisition of ca. 10 Hz during HV conditioning.

A Cockcroft-Walton HV power supply (HVPS) is installed in a tank filled with pressurized SF_6 gas. The output of the HVPS is connected to the HV terminal of the segmented insulator through an output resistor. A 100 MΩ output resistor is used for HV conditioning and generation of a low-current beam. A 67 kΩ output resistor is employed for generation of a high-current beam such as 1 mA, so that the HV drop across the resistor is reasonably small for high current operation and as large as possible to avoid damage of the HV power supply in case of discharge. A 5 GΩ external resistor is connected to the segmented insulator in parallel, so that the output voltage of the HVPS is 510 kV when 500 kV is applied to the insulator during HV conditioning and low-current operation, while the output voltage of the HVPS is almost 500 kV for high-current operation. Reported throughout, the voltage value is the voltage applied to the insulator unless otherwise specified.

III. OPERATION AT THE cERL OF KEK

A. Operation of eight-segment insulator

After generating 500 keV beam at JAEA, high voltage testing was performed with the central stem electrode removed, to benchmark high voltage performance prior to shipment of the gun to KEK. The gun very quickly reached 539 kV for 3.5 hours, as shown in Fig. 2(a). The cross-sectional configuration of the insulator for this measurement is shown in Fig. 2(d). After installation of the gun to the cERL at KEK, another HV test was performed with the same gun configuration. However, this time discharges were suffered at 422 kV and higher voltage could not be reached, as shown in Fig. 2(b). Black and brown dots were found on the inside surfaces of the white ceramic of the top and bottom segments during installation of the gun; therefore, it was speculated that these two segments of the insulator were damaged for some unknown reason. Gun operation with eight segments and with the top and bottom ceramics short-circuited led to stable application of 431 kV, as shown in Fig. 2(c). The gun configuration is schematically shown in Fig. 2(e). It was decided to limit the maximum gun operational voltage to 390 kV for operation with only the eight segments, taking a 40 kV safety margin into consideration. Operation at 390 kV was performed since April 2012 for four years.

The gun was typically operated from 12:00 to 23:00 on weekdays during the beam commissioning time. The stability of the gun HV was excellent and no HV breakdown event due to the gun itself was observed. High stability of gun operation is indispensable for future industrial applications such as EUV lithography [5]. The gun vacuum pressure during operation is 8×10^{-10} Pa. The average beam current at the cERL was gradually increased from 1 to 100 μA while

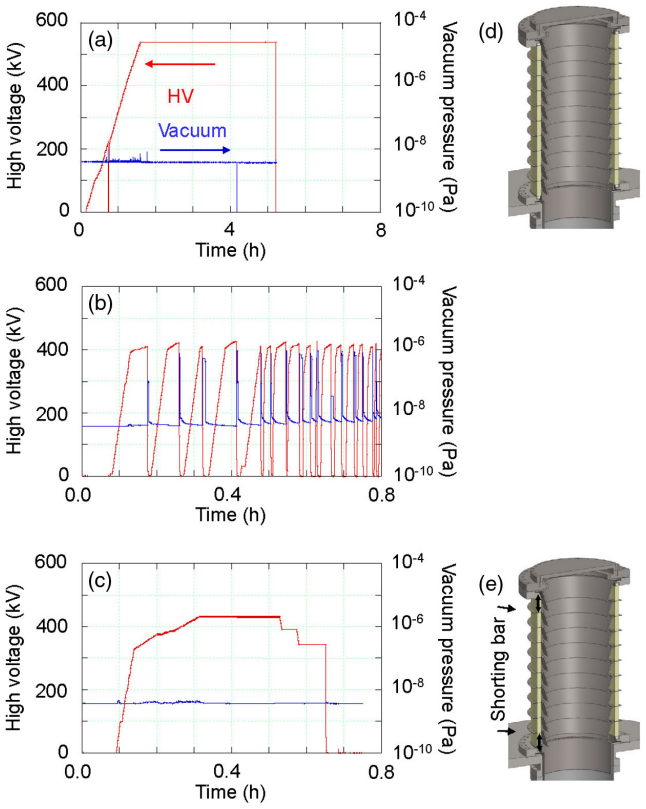

FIG. 2. HV testing without the central stem electrode. HV (red curve) and vacuum pressure (blue curve) as a function of time measured (a) at JAEA and (b) at the cERL just after installation of the gun. The insulator configuration for both measurements is given in (d). HV and vacuum pressure at the cERL with top and bottom segments short-circuited (c). The insulator configuration is given in (e).

monitoring radiation level outside the accelerator hall. Besides commissioning the cERL accelerator complex, the electron beam at the cERL was used for such applications as generation of a narrow-band x-ray beam via laser Compton scattering (LCS) for x-ray fluorescence measurements [20]. The quantum efficiency of the GaAs photocathode at 530 nm ranged from 4% to 12% during the LCS experiment which ran from January to July in 2015 (see Fig. 3). The 1/e lifetime was 6000 h, which was sufficient for the LCS experiment, although the charge extracted was only 6 C. The cathode lifetime study at the cERL will be continued with elevated beam current.

The maximum average current generated to date at the cERL was 0.9 mA demonstrated in March 2016. Figure 4 shows the operational status of the gun for a day during generation of a >0.8 mA beam. The HV and vacuum pressure of the gun chamber were 390 kV and 1×10^{-9} Pa during operation, respectively. The recirculated beam current (green curve) is measured at the beam dump placed downstream of the main accelerator. The quantum efficiency (QE) of the GaAs photocathode (purple curve) is derived from the beam dump current and the monitored

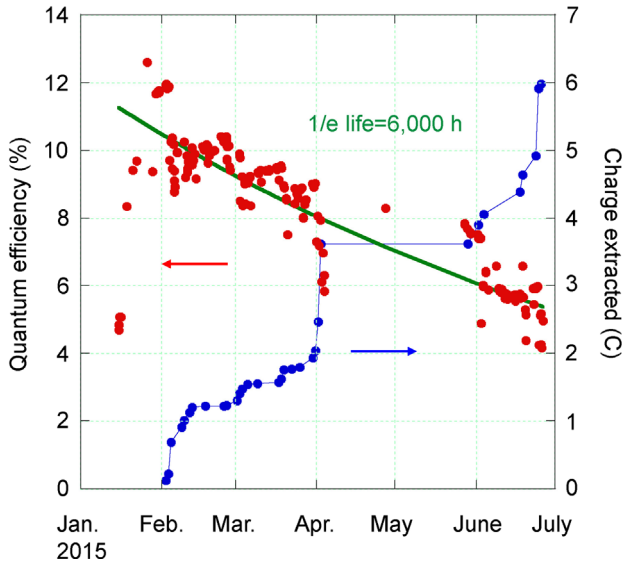

FIG. 3. Quantum efficiency of GaAs photocathode (red circle) and charge (blue circle) extracted during the low current cERL commissioning from January to July in 2015.

laser power at the laser room. The beam generation of >0.8 mA continued for almost 6 h and the charge extracted was 25 C. During this experiment, the GaAs wafer was untouched and no additional activation process for the GaAs surface such as recesiation was performed. The QE dropped rapidly just after beam generation and then stayed almost constant during >0.8 mA operation. The QE then recovered after beam generation was halted. We cannot explain the reason for the QE behavior at this time, but such a change of the QE has always been observed at the cERL. The extraction charge life cannot be derived from Fig. 4, and measurement of QE degradation with beam currents greater than 1 mA will be required. In summary, the gun delivered a stable beam to the cERL at 390 kV for more than four years without trouble.

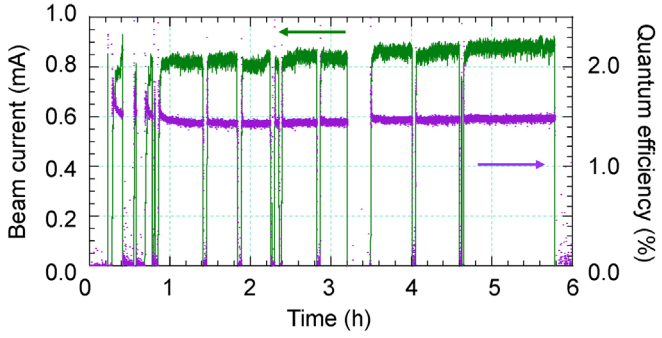

FIG. 4. Operational status of the gun during >0.8 mA beam generation. The green and purple curves show the beam dump current and quantum efficiency of the GaAs photocathode, respectively, as a function of time.

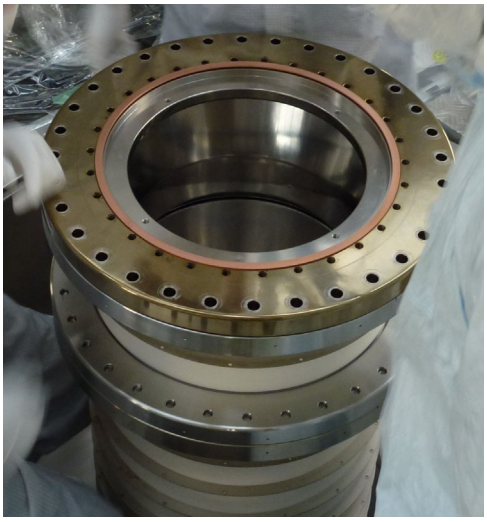

FIG. 5. Photograph of the two-segment insulator on the top of the existing ten-segment insulator.

B. Eight- plus two-segment insulator

To recover the 500 kV operation, a new two-segment insulator was prepared [15]. The dimensions and materials of each segment were the same as those of the original ten-segment insulator. The size of each segment is 400 mm outer diameter, 360 mm inner diameter, and 65 mm in height. The insulator ceramics consists of 99.8% aluminum oxide Al_2O_3 (A99P, Shinagawa Fine Ceramics). The silver brazing between the Kovar ring and stainless steel ring end flange was performed by Hitachi Power Semiconductor Device. The guard rings to protect the ceramics from field emission are made of titanium and their mechanical design is similar to those of the original guard rings. The two-segment insulator was installed on the top of the existing insulator, the original configuration of which remained the same [15], as shown in photograph of Fig. 5. The total length of the output resistor was shortened from 500 mm to 350 mm to provide sufficient space for installation of the additional two-segment insulator, because the HVPS, the output resistor and the insulator are connected in series inside the SF_6 tank (see Ref. [12]).

Figure 6 shows the HV conditioning of the eight- plus two-segment insulator without the central stem electrode. Operation at 539 kV was reached within 1 h, without observation of any discharge activity, which is better than initial tests at JAEA shown in Fig. 2(a) and indicates that installation of the two-segment insulator itself was successful.

Figure 7 shows a cutaway schematic of the gun with the additional two-segment insulator and guard rings. The configuration is similar to that of Fig. 1, except for the additional insulator segments and extension of the stem electrode. Figure 8 shows Poisson [21] electrostatic field maps of both gun configurations. The left and right correspond to the original ten-segment insulator and the

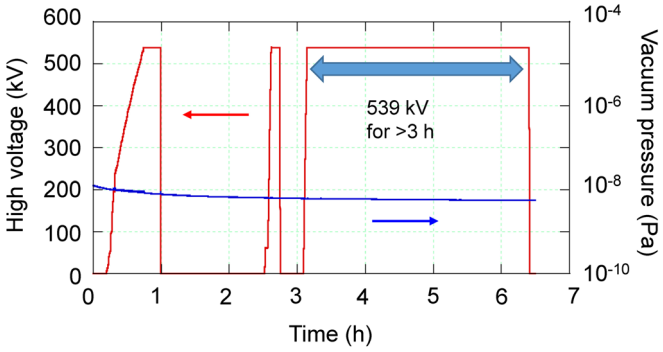

FIG. 6. HV testing for eight- plus two-segment insulator without central stem electrode.

eight- plus two-segment insulator, respectively. Figures 8(a) and 8(d) show the surface electric fields of the inner stem electrode as a function of z along the central axis of the insulator. The origin of z is the center of the cathode.

When the additional two-segment ceramic insulator was installed, the central stem also required extension. Initially, an extension tube was bolted to the original stem. When biased at 500 kV, the maximum electric field of the stem was 9.5 MV/m near $z = 300$ mm, where the extension tube was bolted and the maximum field on the guard ring was 10 MV/m near $z = 500$ mm. However, frequent discharge occurred at 180 kV, although the maximum field

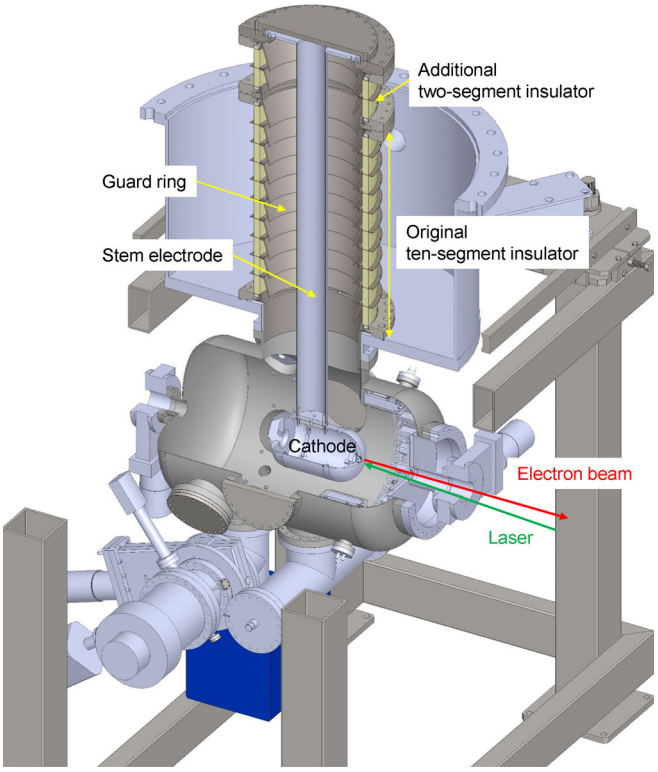

FIG. 7. Schematic illustration of the 500 kV dc photoemission gun at the cERL with additional two-segment ceramic insulator installed.

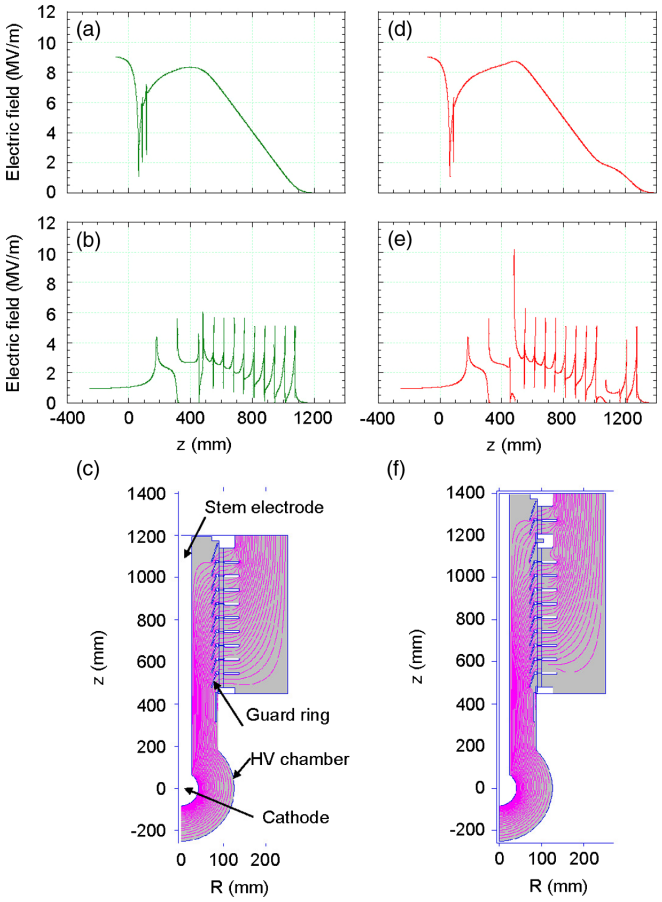

FIG. 8. Field distributions of the inner stem electrode, outer guard rings, and HV chamber for the original ten-segment insulator (left side) and the eight- plus two-segment insulator (right side). (a) and (d) Surface electric fields of the inner stem electrode at 500 kV as a function of z. (b) and (e) Surface electric fields of the outer anode chamber and guard rings at 500 kV as a function of z. (c) and (f) Field distributions inside the gun chamber.

of the stem was small and estimated to be 3.4 MV/m. A radiation survey clearly showed that the field emission was generated from the connection between the original stem and the extension tube. However, the reason for the frequent discharge at such low voltage remains unclear.

Replacement of the original stem with a longer stem without the bolted connection helped to decrease the stem electric field near $z = 300$ mm, as well as the peak field of the guard ring. With this longer stem, 400 kV could be applied without discharge and typical conditioning processes could be continued. The surface electric fields of the inner stem electrode and the outer anode chamber at 500 kV are shown in Figs. 8(d) and 8(e) as a function of z, respectively. A comparison of Figs. 8(a), 8(b), and 8(d), 8(e) indicates that both cathode and anode electric fields of the new configuration with the eight- plus two-segment ceramic insulators were greater than those with the original ten-segment insulator. For the new configuration,

the stem field around $z = 500$ mm was 9 MV/m at 500 kV and that of the guard ring was around 10 MV/m at 500 kV, while the maximum cathode and anode fields were 8.5 MV/m and 6 MV/m, respectively, for the original configuration.

C. Gun conditioning and HV threshold for stable operation

A dc high voltage photoemission gun can be operated without discharge at HV below the threshold voltage, which corresponds to the minimum voltage where discharge ceases during HV conditioning. Figure 9(a) shows a typical conditioning process. The red and blue curves show the HV and vacuum pressure as a function of time, respectively. At cERL, the HVPS is interlocked by the radiation monitors and the vacuum gauges during HV conditioning to protect the gun system. Typical set values of the interlock system were 1×10^{-5} Pa for vacuum and 1000 μSv/h for radiation. Figure 9(b) shows an enlargement of Fig. 9(a) for a typical discharge. When discharge occurs at a set-point HV value, the discharge current is drawn from the HVPS. If the discharge current exceeds the capacity of the HVPS, then the HV becomes smaller than the set-point value. When discharge ceases by a drop of the HV, the HV returns back to the set-point value. We defined the set-point HV as the discharge start voltage and the HV where discharge ceases as the discharge stop voltage. The vacuum pressure increased upon discharge and decreased when the discharge ceased. The time delay for the increase of the vacuum pressure against discharge was attributed to the time constant of the vacuum gauge.

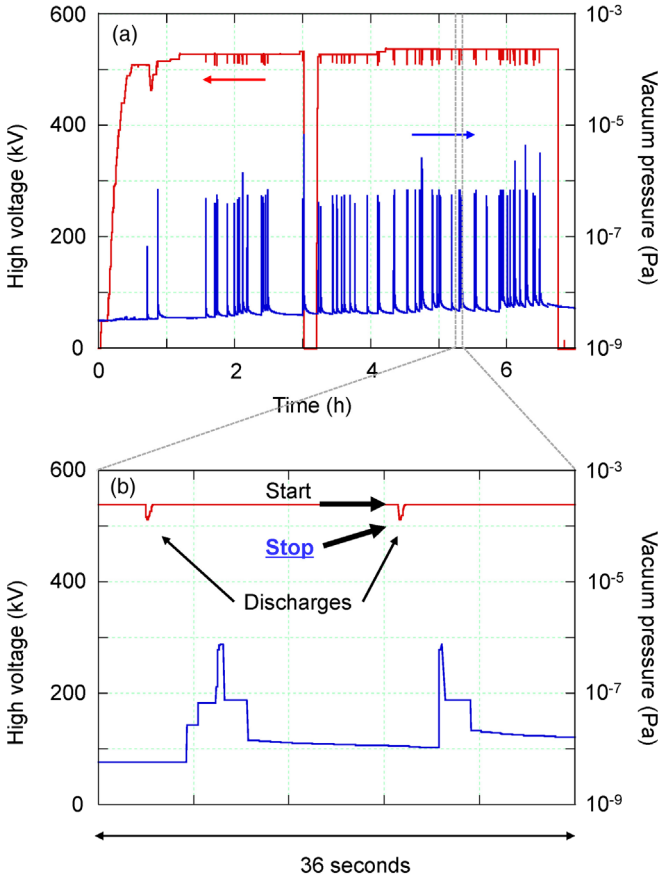

FIG. 9. (a) Typical HV conditioning as a function of time for 1 day. The HV is shown by the red curve and vacuum pressure is shown by blue curve. An enlargement of the time slot shown in (a) is plotted in (b). When discharge occurs, the HV drops and vacuum pressure rises. Discharge start and stop voltages are shown by thick black arrows.

Figure 10(a) shows the proposed avalanche discharge model based on the interplay between electron stimulated desorption (ESD) from the anode surface and subsequent secondary electron emission from the cathode by the impact of ionic components of the ESD molecules or atoms. The field emission can be generated from the cathode, and its energy is determined by the set-point

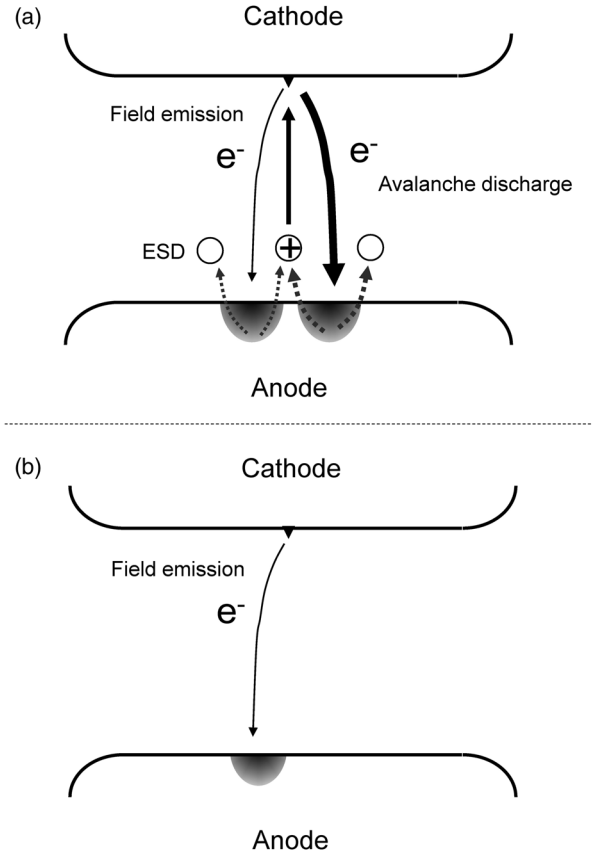

FIG. 10. (a) Avalanche discharge model. The field emission electrons generated from the cathode penetrate the anode surface layer, which results in electron stimulated desorption (ESD). A part of ESD is ionized and accelerated back to the cathode, which leads to the generation of secondary electron emission. The interplay between ESD and subsequent secondary electron emission can induce avalanche discharge. (b) When the electron beam energy is low, the source of ESD has been removed and discharge does not occur.

HV value. The field emission electrons can penetrate the anode with a penetration depth determined by the electron energy, and ESD from the anode surface is induced. A part of the ESD is ionized and accelerated back to the cathode surface, which results in secondary electron emission. This interplay between ESD and secondary electron emission yields an avalanche discharge. When the energy of the field emission electrons decreases, the penetration depth of the electron also decreases, which leads to a reduction in the amount of ESD and a halt of the avalanche discharge process, as shown by Fig. 10(b). When the molecules and atoms adsorbed on the anode surface layer with a depth that corresponds to the applied HV are completely desorbed, the interplay between ESD and secondary electron emission does not occur and the HV can be applied without avalanche discharge. This is the HV threshold voltage. The threshold voltage increases with the number of discharges as the molecules and atoms adsorbed on the surface layer are removed.

The HV threshold for stable operation of the dc photoemission gun during the conditioning process of the eight- plus two-segment ceramic insulators was determined [16]. Figure 11 shows the gun conditioning results as a function of accumulated HV application time. The HV, the vacuum pressure, and radiation are given by red, blue, and purple curves, respectively. The time of 155 h is the end of the conditioning described in Ref. [16]. The threshold voltage was 494 kV due to the limited conditioning time in Ref. [16]. After the HV threshold was determined, the output resistor of the gun was replaced from 100 MΩ to 67 kΩ for high-current operation at the cERL. After demonstration of >0.8 mA operation at 390 kV and beam generation at 450 kV, the output resistor was returned back to 100 MΩ. A further 50 h of conditioning was performed for 500 kV operation, as shown in Fig. 11.

The red pluses and blue crosses in Fig. 12 show the discharge start and stop voltages, respectively, as a function of the number of discharges. The threshold voltage, which corresponds to the minimum discharge stop voltage, was 494 kV after 2400 discharges (see Fig. 12). At this point, the high voltage conditioning resistor was replaced for high current operations. Approximately 200 hours of beam delivery occurred at voltages 390 and 450 kV, which are well below the 494 kV threshold voltage. The conditioning resistor was reinstalled and the threshold voltage was found to jump to 501 kV at the beginning of extra conditioning (see Fig. 12(b)) although no discharge happened during the beam delivery. This indicates application of HV even below the threshold voltage contributes to an increase of the threshold level. The proposed discharge model explains the mechanism as follows. A small dark current below the detection threshold would be drawn from the cathode to the anode chamber. This undetectable dark current induces ESD, which results in the removal of molecules and atoms adsorbed on the anode surface layer. Further conditioning processes were continued and the threshold voltage reached 510 kV, which well exceeded the 500 kV necessary for 500 keV electron beam generation. The discharge stop voltage slowly increased, even if the discharge start voltage was set to 539 kV, which is the maximum voltage determined by the HVPS.

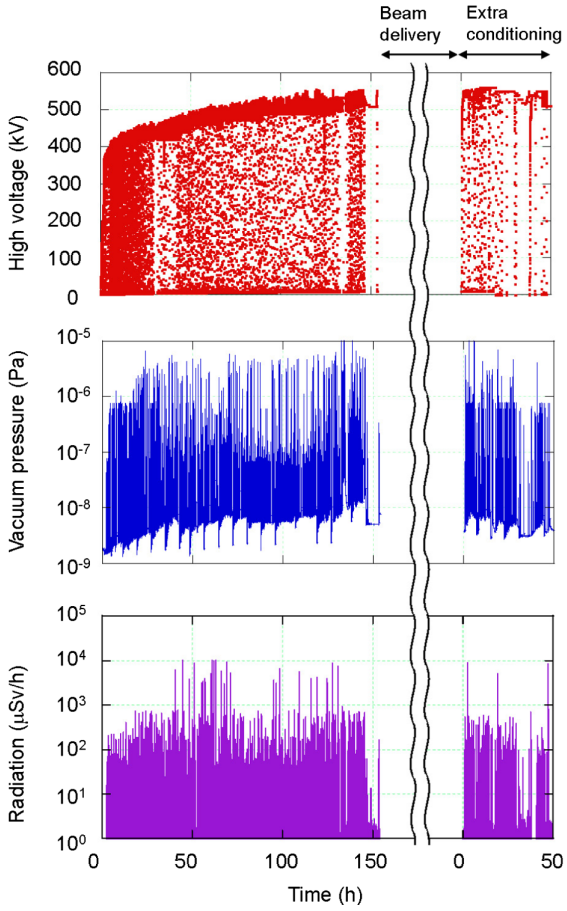

FIG. 11. Gun conditioning results as a function of integrated time for eight- plus two-segment insulator with cathode in place. The HV, the gun vacuum pressure, and the radiation are represented by red, blue, and purple curves, respectively. Approximately 200 h of beam delivery occurred at voltages 390 and 450 kV after 155 h of conditioning. Then extra gun conditioning was performed for 50 h.

Since performing this conditioning, we have not experienced any discharge event at 500 kV, once the threshold HV exceeds 500 kV. Our early observation described in Ref. [16], that the gun can be operated stably with no discharge below the threshold HV, has been confirmed again at the higher voltage.

D. Dark current measurement

Dark current from the gun is undesirable from a stable operation perspective. Particularly for continuous wave (cw) electron accelerators, dark current may be accelerated and cause damage to accelerator components. For rf guns,

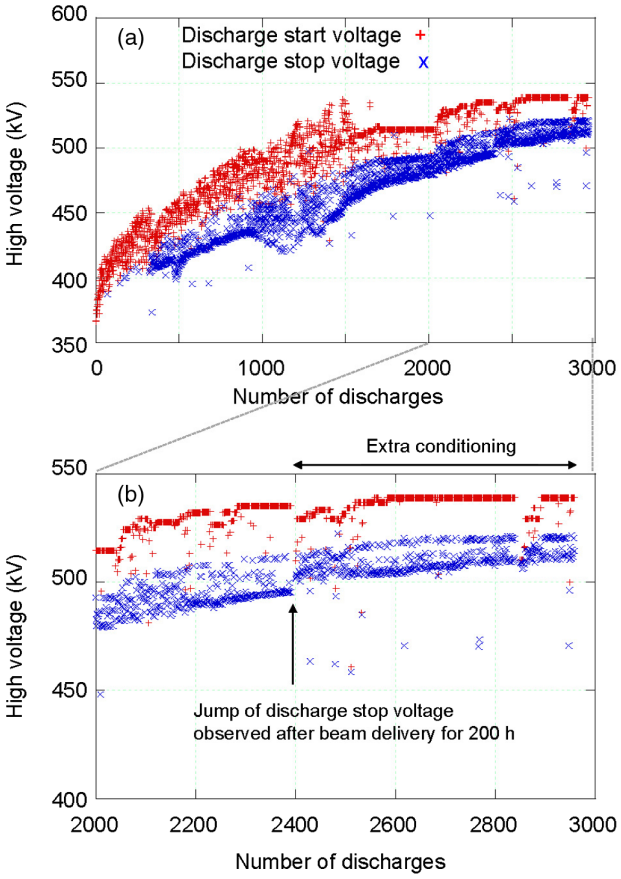

FIG. 12. (a) Discharge start (red plus) and stop (blue cross) voltages as a function of the number of discharges. (b) Enlargement from discharges 2000 to 3000. Discharge stop voltage jumped to 501 kV at the beginning of extra conditioning after beam delivery for 200 h.

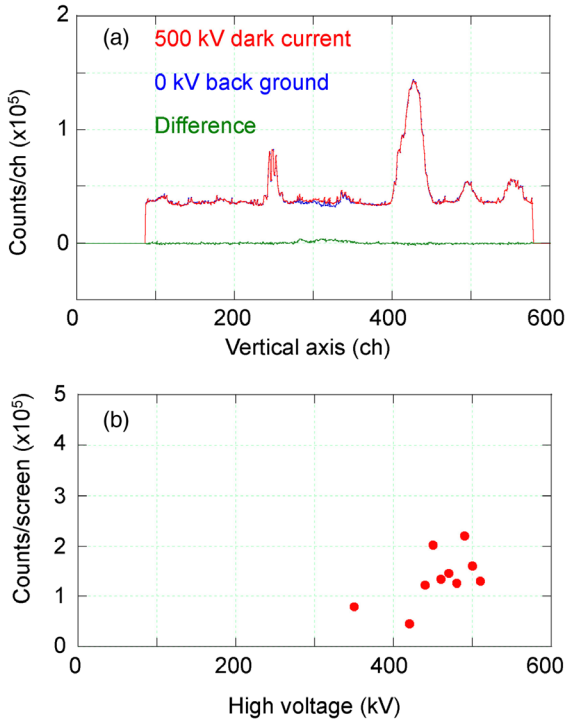

FIG. 13. (a) Dark current profile at 500 kV (red curve) measured on a YAG screen placed 1 m downstream from the photocathode and background profile at 0 kV (blue curve). The exposure time of the camera is 3 s. The green curve shows the difference of the blue curve and the red curve. (b) Areal sum of the green profile as a function of HV (red solid circles).

a large amount of dark current is observed because the surface electric field is much greater than that of dc guns. The average dark current from a normal conducting rf gun at Los Alamos National Laboratory is 70 μA [22]. A superconducting rf photoinjector at Rossendorf shows nanoampere levels of dark current [23,24]. Although the dark current from the Advanced Photo-injector EXperiment (APEX) warm rf gun at the Lawrence Berkeley National Laboratory was measured to be greater than nanoampere level [25], a recent study showed the dark current was 0.1 nA at 750 keV [26].

Dark current can be detected by radiation monitors or beam profile monitors. No dark current was observed in the present gun by radiation monitors when a metal dummy puck was installed on the cathode at 500 kV. When a Mo puck on which a GaAs wafer was indium-sealed was mounted on the cathode, a subtle increase of the radiation monitor signal was observed. It was thus concluded that the source of radiation was the Mo puck with the GaAs wafer.

The beam profile of dark current on a YAG screen placed 1 m downstream from the photocathode was measured to estimate the amount of dark current. The exposure time of the camera was set to 3 s for dark current measurement. The projections on the vertical axis of dark current profiles at 500 kV and the background at 0 kV are shown in Fig. 13(a), where the red curve is the dark current at 500 kV, the blue curve is the background at 0 kV, and the green curve is the difference of the background from the dark current signal. Figure 13(b) shows the net amount of dark current obtained after subtraction as a function of HV. Although the dark current increases slightly with the HV, it does not seem to increase exponentially. Therefore the source of dark current would not be field emission.

The YAG screen intensity versus beam current was calibrated with a 500 keV electron beam. The beam profile of the 500 keV electron beam on the screen is shown in Fig. 14(a). The projection on the vertical axis is shown in Fig. 14(b). The electron beam current was measured with a Faraday cup placed just downstream of the screen. The peak current of the electron beam was 0.692 mA with a macropulse duration of 0.1 μs at a repetition rate of 5 Hz. The exposure time of the camera was 0.01 s and the area of the projection corresponded to an electron beam charge of 0.0692 nC if the amount of fluorescence is assumed to be independent on electron beam energy. Based on these measurements, the dark current is assumed to be less than 2.7 pA. During this measurement, the vacuum gauge of the electron gun was switched off. When the vacuum

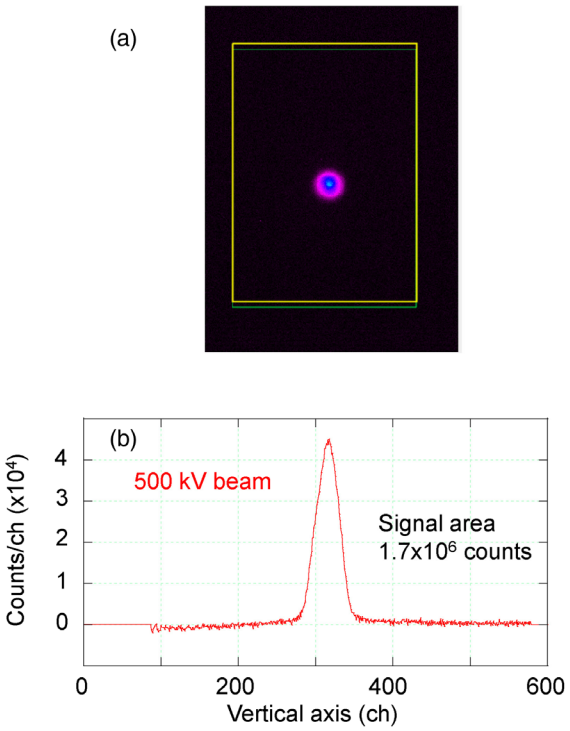

FIG. 14. (a) Measured profile of 500 keV electron beam to calibrate the signal intensity on the screen. (b) Projection of the vertical axis. The electron beam charge for the screen shot is 0.0692 nC.

gauge was switched on, the dark current generated from the photocathode with QE of a few percent was roughly 50 pA. The gun vacuum gauge was used to monitor the gun vacuum during the cERL commissioning. The dark current became large when the puck was not properly mounted on the puck holder of the cathode.

IV. OPERATION AT 500 kV

The gun HV was stable at 500 kV during the cERL beam commissioning for many hours with the macropulse average current of 0.3 mA and macropulse length of 0.1 μs at a repetition rate of 5 Hz. The gun vacuum pressure remained less than 8×10^{-10} Pa. The radiation level increased to 0.2 μSv/h due to a small amount of dark current when 500 kV was applied, as described in Sec. III D.

Generation of a high-current beam greater than 0.8 mA at 500 kV for approximately 2 h was demonstrated, as shown in Fig. 15. The red and green curves show HV and the recirculated beam current measured at the beam dump, respectively. We will increase the beam current up to 10 mA, which is the maximum limited by the present capacity of our HVPS.

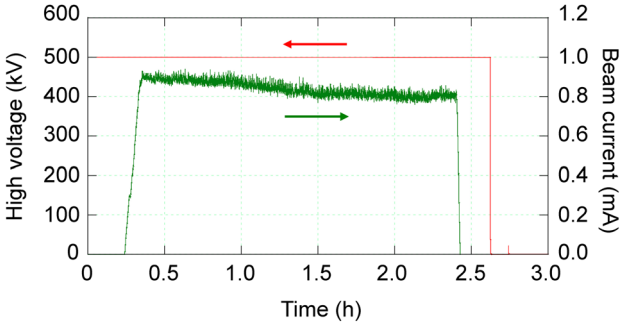

FIG. 15. Operational status of the gun during beam generation at >0.8 mA. The red and green curves show HV and the beam dump current, respectively, as a function of time.

V. SUMMARY

We have presented operational experience of a 500 kV photoemission gun at the cERL of KEK. The gun with an eight- plus two-segment insulator configuration has delivered stable 500 keV beam with a small dark current of a few picoamperes. A maximum beam current of 0.9 mA was generated from the gun and recirculated in the downstream ERL loop. Stable generation of a 500 keV beam with current greater than 0.8 mA was demonstrated for more than 2 h. We will attempt to increase the beam current up to 10 mA.

ACKNOWLEDGMENTS

We would like to express our gratitude to all members of the cERL development group for their continuous support for the construction and operation of the cERL. This work was partially supported by JSPS KAKENHI Grants No. JP15H03594 and No. JP16K05385.

[1] A. Accardi *et al.*, Electron Ion Collider: The Next QCD Frontier - Understanding the glue that binds us all, arXiv:1212.1701.
[2] E. C. Aschenauer *et al.*, eRHIC design study: An Electron-Ion Collider at BNL, arXiv:1409.1633.
[3] J. L. Abelleira Fernandez *et al.* (LHeC Study Group), Report on the physics and design concepts for machine and detector, J. Phys. G **39**, 075001 (2012).
[4] G. H. Hoffstaetter *et al.*, CBETA design Report, Cornell-BNL ERL test accelerator, arXiv:1706.04245.
[5] N. Nakamura, R. Kato, T. Miyajima, M. Shimada, T. Hotei, and R. Hajima, S2E simulation of an ERL-based high-power EUV-FEL source for lithography, in *Proceedings of IPAC 2017, Copenhagen, Denmark, 2017* (JACoW, Geneva, Switzerland, 2017), p. 894.
[6] C. Gulliford, A. Bartnik, I. Bazarov, B. Dunham, and L. Cultrera, Demonstration of cathode emittance dominated high bunch charge beams in a DC gun-based photoinjector, Appl. Phys. Lett. **106**, 094101 (2015).
[7] B. Dunham *et al.*, Record high-average current from a high-brightness photoinjector, Appl. Phys. Lett. **102**, 034105 (2013).

[8] F. Sannibale *et al.*, Advanced photoinjector experiment photogun commissioning results, Phys. Rev. ST Accel. Beams **15**, 103501 (2012).

[9] I. V. Bazarov and C. K. Sinclair, Multivariate optimization of a high brightness dc gun photoinjector, Phys. Rev. ST Accel. Beams **8**, 034202 (2005).

[10] M. Akemoto *et al.*, Construction and commissioning of the compact energy-recovery linac at KEK, Nucl. Instrum. Methods Phys. Res., Sect. A **877**, 197 (2018).

[11] N. Nishimori, R. Nagai, S. Matsuba, R. Hajima, M. Yamamoto, Y. Honda, T. Miyajima, H. Iijima, M. Kuriki, and M. Kuwahara, Generation of a 500-keV electron beam from a high voltage photoemission gun, Appl. Phys. Lett. **102**, 234103 (2013).

[12] R. Nagai, R. Hajima, N. Nishimori, T. Muto, M. Yamamoto, Y. Honda, T. Miyajima, H. Iijima, M. Kuriki, M. Kuwahara, S. Okumi, and T. Nakanishi, High-voltage testing of a 500-kV dc photocathode electron gun, Rev. Sci. Instrum. **81**, 033304 (2010).

[13] N. Nishimori, R. Nagai, S. Matsuba, R. Hajima, M. Yamamoto, Y. Honda, T. Miyajima, H. Iijima, M. Kuriki, and M. Kuwahara, Experimental investigation of an optimum configuration for a high-voltage photoemission gun for operation at ≥500 kV, Phys. Rev. ST Accel. Beams **17**, 053401 (2014).

[14] H. Sakai, E. Cenni, K. Enami, T. Furuya, M. Sawamura, K. Shinoe, and K. Umemori, Field emission studies in vertical test and during cryomodule operation using precise x-ray mapping system, Phys. Rev. Accel. Beams **22**, 022002 (2019).

[15] N. Nishimori, Review of experimental results from high brightness dc guns: Highlights in FEL applications, in *Proceedings of FEL2015, Daejeon, Korea, 2015* (JACoW, Geneva, Switzerland, 2015), p. 269.

[16] M. Yamamoto and N. Nishimori, High voltage threshold for stable operation in a dc electron gun, Appl. Phys. Lett. **109**, 014103 (2016).

[17] N. Nishimori, R. Nagai, M. Yamamoto, Y. Honda, T. Miyajima, H. Iijima, M. Kuriki, M. Kuwahara, S. Okumi, T. Nakanishi, and R. Hajima, Development of a 500-kV photocathode dc gun for ERLs, J. Phys. Conf. Ser. **298**, 012005 (2011).

[18] H. Kurisu, G. Kimoto, H. Fijii, K. Tanaka, S. Yamamoto, M. Matsuura, K. Ishizawa, T. Nomura, and N. Murashige, Outgassing properties of chemically polished titanium materials, J. Vac. Soc. Jpn. **49**, 254 (2006) (in Japanese); H. Kurisu, T. Muranaka, N. Wada, S. Yamamoto, M. Matsuura, and M. Hesaka, Titanium alloy material with very low outgassing, J. Vac. Sci. Technol. A **21**, L10 (2003).

[19] F. Furuta, T. Nakanishi, S. Okumi, T. Gotou, M. Yamamoto, M. Miyamoto, M. Kuwahara, N. Yamamoto, K. Naniwa, K. Yasui, H. Matsumoto, M. Yoshioka, and K. Togawa, Reduction of field emission dark current for high-field gradient electron gun by using a molybdenum cathode and titanium anode, Nucl. Instrum. Methods Phys. Res., Sect. A **538**, 33 (2005).

[20] T. Akagi, A. Kosuge, S. Araki, R. Hajima, Y. Honda, T. Miyajima, M. Mori, R. Nagai, N. Nakamura, M. Shimada, T. Shizuma, N. Terunuma, and J. Urakawa, Narrow-band photon beam via laser Compton scattering in an energy recovery linac, Phys. Rev. Accel. Beams **19**, 114701 (2016).

[21] J. H. Billen and L. M. Young, Los Alamos National Laboratory Report No. LA-UR-96-1834, 1996, https://laacg.lanl.gov/laacg/services/download_sf.phtml.

[22] D. C. Nguyen, N. A. Moody, H. L. Andrews, G. Bolme, L. J. Castellano, C. E. Heath, F. L. Krawczyk, S. I. Kwon, R. McCrady, F. A. Martinez, P. Marroquin, M. Prokop, R. M. Renneke, P. Roybal, W. T. Roybal, T. L. Tomei, P. A. Torrez, W. M. Tuzel, and T. Zaugg, End-point energy measurements of field emission current in a continuous-wave normal-conducting rf injector, Phys. Rev. ST Accel. Beams **14**, 030704 (2011).

[23] R. Xiang, A. Arnold, H. Buettig, D. Janssen, M. Justus, U. Lehnert, P. Michel, P. Murcek, A. Schamlott, Ch. Schneider, R. Schurig, F. Staufenbiel, and J. Teichert, Cs_2Te normal conducting photocathodes in the superconducting rf gun, Phys. Rev. ST Accel. Beams **13**, 043501 (2010).

[24] R. Xiang, A. Arnold, T. Kamps, P. Lu, P. Michel, P. Murcek, H. Vennekate, G. Staats, and J. Teichert, Experimental studies of dark current in a superconducting rf photoinjector, Phys. Rev. ST Accel. Beams **17**, 043401 (2014).

[25] R. Huang, D. Filippetto, C. F. Papadopoulos, H. Qian, F. Sannibale, and M. Zolotorev, Dark current studies on a normal-conducting high-brightness very-high-frequency electron gun operating in continuous wave mode, Phys. Rev. ST Accel. Beams **18**, 013401 (2015).

[26] F. Sannibale *et al.*, Status, plans and recent results from the APEX project at LBNL, in *Proceedings of FEL2015, Daejeon, Korea, 2015* (JACoW, Geneva, Switzerland, 2015), p. 81.